IEEE Photonics Journal
An IEEE Photonics Society Publication

VLC Using 800-μm Diameter APD Receiver Integrated in Standard 0.35-μm BiCMOS Technology

Volume 13, Number 1, February 2021

D. Milovančev, *Member, IEEE*
T. Jukić
N. Vokić, *Member, IEEE*
P. Brandl
B. Steindl
H. Zimmermann, *Senior Member, IEEE*

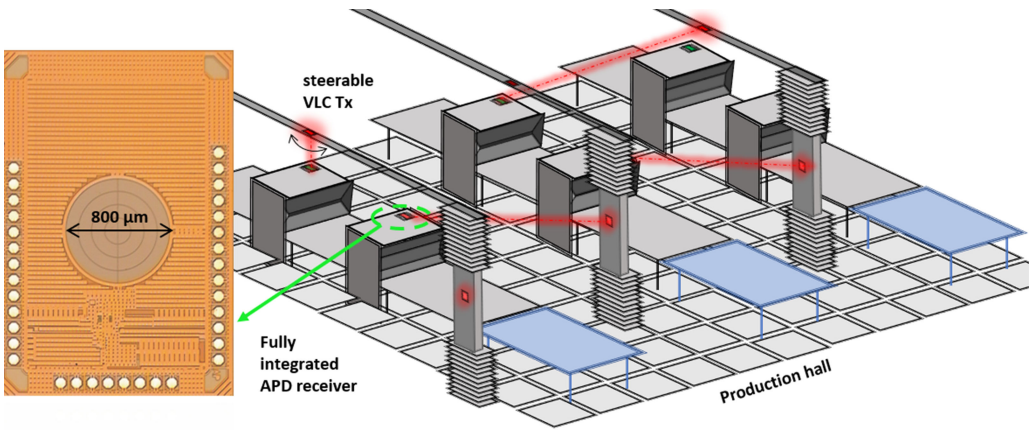

DOI: 10.1109/JPHOT.2020.3036549

VLC Using 800-μm Diameter APD Receiver Integrated in Standard 0.35-μm BiCMOS Technology

D. Milovančev, *Member, IEEE*, T. Jukić, N. Vokić, *Member, IEEE*, P. Brandl, B. Steindl, and H. Zimmermann, *Senior Member, IEEE*

Institute of Electrodynamics, Microwave and Circuit Engineering, Gusshausstrasse, 25/E354 1040, Vienna, Austria

DOI:10.1109/JPHOT.2020.3036549

Manuscript received September 15, 2020; revised October 18, 2020; accepted November 3, 2020. Date of publication November 6, 2020; date of current version January 13, 2021. This work was supported by TU Wien Bibliothek through its Open Access Funding Programme. Corresponding author: H. Zimmermann (e-mail: horst.zimmermann@tuwien.ac.at).

Abstract: The fully integrated 800 μm. diameter avalanche photodiode optical receiver is implemented in 0.35 μm BiCMOS technology without any process modifications. The integrated receiver reaches sensitivities of –33 dBm at 1 Gbit/s and –29.3 dBm at 2 Gbit/s. The reached sensitivities are well within the state-of-the-art of integrated avalanche photodiode receivers and can even be compared to a hybrid avalanche photodiode receiver comprised of high-performing commercial components. The performance of the designed receiver was verified in visible light communication experiments. The receiver could reach up to 16.5 m at 2 Gbit/s and 27 m at 1 Gbit/s of error free transmission distance using a 675-nm point laser source as transmitter. The common indoor illuminance levels up to 500 lux could be tolerated when pointed directly towards the receiver. High sensitivity and high speed make this integrated receiver suitable for future optical wireless communication systems, where due to its integrated nature the manufacturing cost can be lowered, and at the same time the design is compact in size and easy to assemble and scale. Furthermore, no optics is used in front of the receiver due to its large area resulting in a wide field of view.

Index Terms: VLC, avalanche photodiodes, integrated optoelectronics.

1. Introduction

The constant increase of mobile data traffic and excessive use of highly networked devices highlight the need for high-speed enabling technologies. In the next decade it is envisioned that the mobile traffic will increase 1000 times per area and number of connected devices will increase from 10 to 100 times [1]. To evade the inevitable spectrum crunch, full usage of available electromagnetic (EM) spectrum must be made. Optical wireless communication (OWC) presents a viable option as a supporting technology to existing wireless systems for both indoor and outdoor communication. The unlicensed bandwidth and potential for high speed make the optical spectrum an attractive option if limited coverage and mobility are to be tolerated. The promising application scenarios would be in electromagnetic interference (EMI) sensitive areas such as hospitals, airplanes, industrial plants or for targeted high-speed consumer operations such as fast and secure high-definition video streaming.

The practical setup and use cases for OWC have been studied thoroughly from system architecture point of view [2], [3]. In [4] the light-fidelity (Li-Fi) concept has been elaborated for indoor communication scenarios such as GigaDock, GigaShower etc. However, specifics of the used devices on a component level have not been tackled in many studies. Usually commercially available components are being used for OWC optical transmitters and optical receivers, assembled on a printed circuit board which results in larger parasitics, footprint and unreliability. In this paper, the attention is dedicated to development of a custom integrated solution for optical receiver intended for visible light communication (VLC). The study in [5] recognized the receiver sensitivity as one of the main challenges for Gbit OWC and pointed out the need for avalanche photodiodes (APD) that have inherent gain mechanism in contrast to their PIN counterparts which are usually a standard option for optical receiver. Additionally, the optical receiver should be easy to assemble, economical and miniaturized [5]. Optoelectronic integration of photonic and electronic components on a single wafer can satisfy these demands. For receiver operating in visible and near infrared range, silicon technology is a natural choice. Of course, the fabrication of photonic and electronic circuitry in the same technology must allow for some performance compromises.

In this paper we will present a fully integrated APD receiver in 0.35 μm BiCMOS technology with large photodiode diameter of 800 μm. To the best of the authors' knowledge, this is the largest active area integrated APD receiver in a standard technology which in addition is fully capable for Gbit operation without the need for segmenting the photodiode as in [6]. Furthermore, the required APD reverse bias voltage is below 60 V, which is significantly lower compared to high performance commercial APDs with biasing voltages usually spanning above 200 V. The large active area of the receiver places its design into VLC perspective since it reduces the needed irradiance for proper operation. The reduced irradiance, depending on the system design, can either translate into higher transmission distance or larger coverage area for a certain transmit optical power. In our previous works [7], [8], the fully integrated APD receivers with diameters of 200 μm and 400 μm were designed in the same technology and used as optical wireless receivers. It was shown that by doubling the diameter of the APD, the error free transmission distance increases close to an estimated value of 1.73 times. However, the APDs of the designed receivers could not achieve maximum bandwidth at optimum APD multiplication gains M. For this reason, the structure of the APD was modified so that at multiplication gains M of practical value, the highest bandwidths can be achieved. The modifications of the APDs did not require any process changes, only the layout of the used process layers was manipulated as described in [9]. To increase the performance gains and examine the limits of technology, the diameter of the used APD was chosen to be doubled with respect to a maximum diameter in a previous design run.

The receiver is tested in a simple indoor VLC setting using a 680 nm narrow beam VCSEL which can be steered via MEMS mirror (described in [10]). The receiver performance in respect to different ambient light sources as well as angular displacement is also evaluated. A possible use case based on achieved error-free communication distances of tens of meters using this lens-free wide angle APD receiver could enable communication over a highly automated production hall with either fixed point laser sources or steerable ones, see Fig. 1.

2. Design of Integrated APD Receiver

The 800-μm diameter APD opto-electronic integrated circuit (800APD OEIC) was realized in a standard 0.35 μm BiCMOS technology requiring no process modifications. To protect electrical circuitry from high APD bias voltage careful layout level steps were implemented such as placing the substrate guard ring at a larger distance than nominal away from the active devices.

2.1 Integrated modulation Doped APD

Integrated APD had the vertical structure shown in Fig. 2(a). The vertical structure is comprised of separate multiplication region (n+/p-well) and absorption region (thick epitaxial layer). The epitaxially grown layer of approximately 12 μm thickness with a P-doped substrate allows high

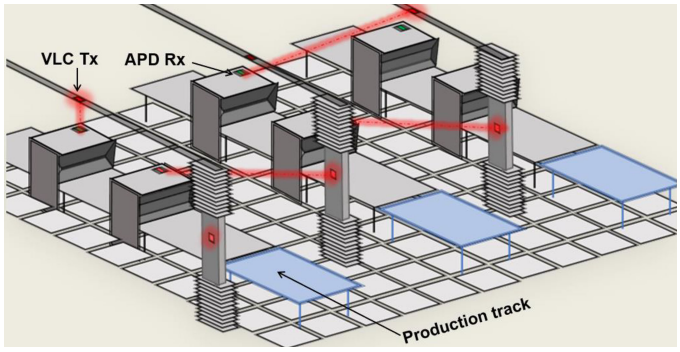

Fig. 1. Automated production hall: possible use case of large area integrated APD receiver ■ and pencil beam visible light laser ■.

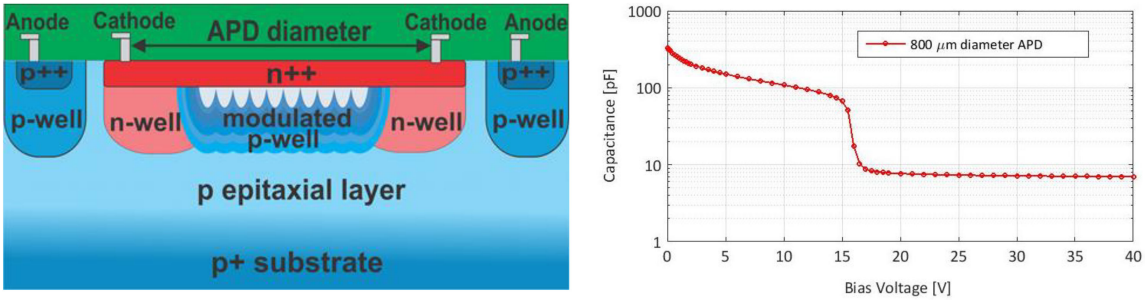

Fig. 2. (a) Integrated APD structure in BiCMOS technology. (b) Measured capacitance of 800 μm APD vs. reverse bias voltage.

quantum efficiency since it serves as the absorption zone for the photodiode. The electrons from the P-doped epitaxial layer are used as the basic generator of the avalanche effect, the charge carriers influenced by the electric field inside absorption zone move vertically into the multiplication zone where due to acceleration they gain enough energy to create new electron-hole pairs by impact ionization. The design of integrated photonics in standard CMOS and BiCMOS technologies is challenging since the doping concentrations of the available wells and substrate are fixed by the used technological process. Therefore, the structure of the APD and its performance are directly influenced by the used technology. The implementation of APDs in the used 0.35 μm BiCMOS technology together with electrical circuitry was studied in previous works, [7], [8], when 200 μm diameter and 400 μm diameter APDs were co-integrated with custom transimpedance amplifiers. These first implementation of APD receivers showed that at the theoretically determined optimum APD multiplication gain M based on the noise of electrical circuitry the intrinsic APD bandwidth was limited. The gain-bandwidth multiplication curve of this APD itself favored high multiplication gains ($M = 65.9$) for a bandwidth of 810 MHz [11] which were not optimum for the low-noise TIA design, since the input referred noise of the TIA should be matched to the APD noise for best performance. To increase the APD bandwidth even at lower multiplication gains, the modulation doped structure was pursued, this technique was first introduced in HV CMOS technology [9]. The layout of p-well was perforated to reduce the effective doping without any process modification. The fill factor of the modulation doped p-well by means of introducing a hole pattern in its layout is 83%. This translated to an increased bandwidth due to different electrical field distribution but at the expense of a higher substrate biasing voltage [12]. The bandwidth increase by effective doping reduction is due to the electric field distribution change between the multiplication zone

TABLE 1
Gain-Bandwidth Properties of the Integrated APDs in 0.35 μm BiCMOS Technology

M	BW	V_{sub}[V]	R [A/W]	λ	APD
8	1.95 GHz	37.0 V	2.96	635 nm	Modulation doped device [12]
20	2.3 GHz	47.5 V	7.4		
80	1.48 GHz	52.2 V	29.6		
61.3	1 GHz	30 V	19	670 nm	Unmodulated device [13]

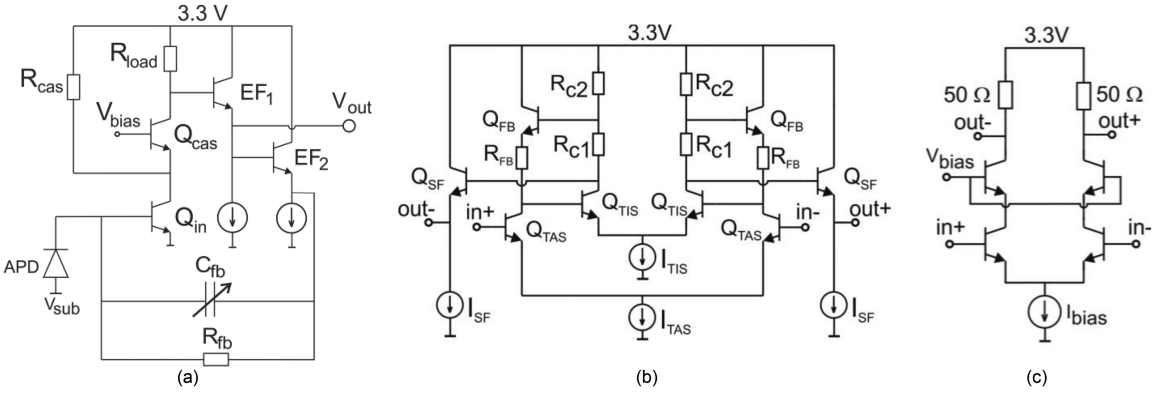

Fig. 3. (a) Cascoded CE TIA. Post-amplifying stages: (b) modified CH amplifier and (c) cascoded 50-Ω output driver.

and the absorption zone in favor of the absorption zone. By having a higher electric field in the absorption zone, the charge carriers can be accelerated up to the saturation speed even at lower multiplication gains. However, these lower multiplication gains now correspond to a higher APD reverse voltage. The measurements on a wafer level of both modulation doped and not modulation doped 100 μm diameter APDs are summarized in [12] and [13], respectively, Table 1 provides their main gain-bandwidth characteristics. It can be seen that electric field distribution in the modulation-doped case favors moderate gains allowing for highest bandwidth in this gain region which is more suitable for TIA integration, and also shows that the maximum achievable bandwidth is 2.25 times larger in the modulation doped device (2.3 GHz) compared to its unmodulated counterpart (1.02 GHz).

Unfortunately, the inhomogeneity of the p-well had as the unexpected consequence the increased APD noise factor F and impact-ionization ratio k_{eff} compared to APDs without modulation doping [14]. This reduced by some margin the sensitivity of our receivers, but VLC performance gains were still achievable. The capacitance of the 800-μm APD was measured to be 7 pF at high substrate voltage, see Fig. 2(b).

2.2 Optical Receiver – Circuit Design

The first stage of optical receiver is the transimpedance amplifier (TIA) stage which sets the limits for the noise and bandwidth performance of the whole receiver. The integrated approach facilitates the design since there are no additional bond wire inductances and bond pad capacitances at the most sensitive node of the receiver, which is the interface between TIA and large-area photodiode. The designed TIA stage has input transistor Q_{in} in common emitter (CE) configuration, but the loading transistor R_{load} is decoupled with a cascode transistor Q_{cas}, thus reducing the Miller effect, see Fig. 3(a). Input transistor had large dimensions due to significant photodiode junction capacitance and required high biasing current.

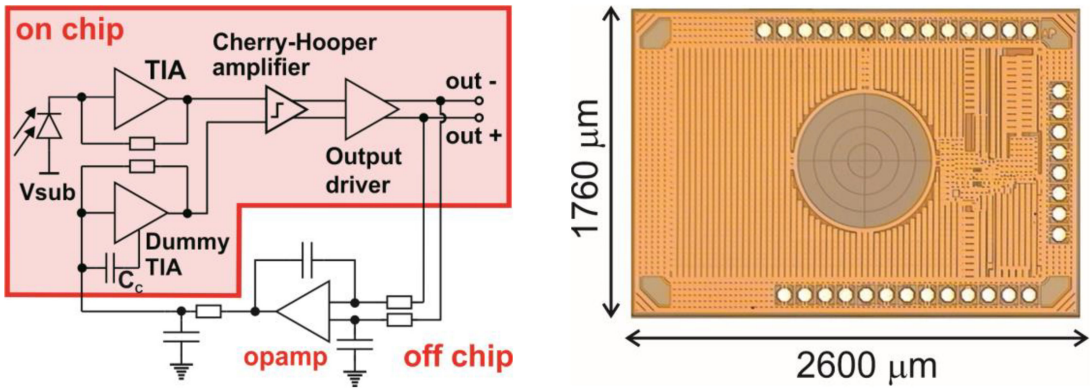

(a) (b)

Fig. 4. (a) Block diagram of the complete optical receiver. (b) Photomicrograph of 800APD OEIC.

An additional path for biasing current is supplied through R_{cas}. In this way the constraints on value of R_{load} and corresponding voltage drop were relaxed. Approximately 22% of Q_{in} biasing current flows through R_{load} and 78% of the biasing current flows through R_{cas}. This design approach was demonstrated first in GaAs MESFET technology in [15]. The feedback resistor R_{fb} had a resistance of 1.3 kΩ. The 3-dB bandwidth and amount of the peaking could be tuned with switchable capacitance C_{fb} (0.35 fF, 70 fF and 105 fF). The variable C_{fb} network was implemented since it was unknown what bandwidth properties the large area photodiode would have. The postlayout simulations of the TIA stage resulted in a bandwidth of 685 MHz when the highest capacitance value $C_{fb} = 105$ fF was applied.

The second post-amplifying stage was a modified Cherry Hooper (CH) stage with emitter followers shown in Fig. 3(b). The topology was first introduced in [16], and the design guidelines were given in [17]. The addition of Rc_1, Rc_2 and source followers improves the gain by approximately $(1+Rc_1/Rc_2)$ compared to a standard Cherry Hooper design. The postlayout simulations show a gain of 21 V/V and a bandwidth of approximately 2 GHz. The last stage in the design is the output driver that drives 50-Ω loads. The cascoded stage is used to reduce the Miller effect of the input transistors, see Fig. 3(c). The biasing current is high ($I_{bias} = 20$ mA) to enable a wide voltage swing across the 50-Ω resistors. The bandwidth of the driver stage equals 2 GHz as well and its voltage gain is 5.4 V/V.

The block diagram and photomicrograph of the complete optical receiver with the abovementioned stages is shown in Fig. 4(a). An offset compensation loop was done off-chip to provide more flexibility and performance security for this initial design, but the version with on-chip offset compensation is also possible, as demonstrated for APD receiver in the same technology [18]. The opamp works as a proportional integral (PI) controller as it senses the voltage offset at the output and provides the adequate input to the replica (dummy) TIA (on-chip). The dummy TIA has the same design as the input TIA, except the compensating capacitor C_C that limits the bandwidth of the dummy TIA thus reducing its noise contribution. The designed chip had an area of 1760 μm $\times$ 2600 μm, see Fig. 4(b). The postlayout simulations of the whole receiving chain resulted in the following values of bandwidth: 900 MHz ($C_{fb} = 0$), 835 MHz ($C_{fb} = 35$ fF), 755 MHz ($C_{fb} = 70$ fF) and 635 MHz ($C_{fb} = 105$ fF).

3. APD Receiver Characterization

The APD receiver characterization was done using a fiber coupled 675-nm laser source for which the responsivity of the photodiode should be quite high and, based on previous studies, a high

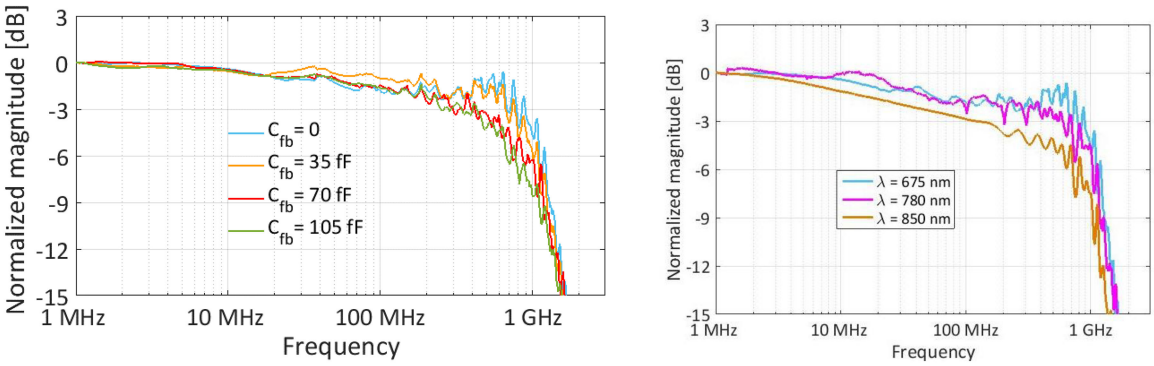

Fig. 5. (a) 800APD OEIC frequency response for different values of Cfb. (b) 800APD OEIC frequency response at different wavelengths λ.

bandwidth should be possible [7], [8]. The level of TIA feedback capacitance was varied during the following measurement.

3.1 Frequency Response

For the frequency response measurements, the laser source was modulated via one port of vector network analyzer VNA and the light was coupled via multimode fiber onto the photodiode´s active area while one of the outputs of the APD receiver was fed to the other port of the VNA. The measured S21 parameter is the frequency response of the 800APD OEIC displayed in Fig. 5(a). The achieved 3-dB bandwidths are 890 MHz ($C_{fb} = 0$), 730 MHz ($C_{fb} = 35$ fF), 520 MHz ($C_{fb} = 70$ fF) and 400 MHz ($C_{fb} = 105$ fF). The substrate voltage was kept at –55 V during the measurements, but the high bandwidths could be sustained down to – 30 V.

The dependence of the bandwidth on the used laser wavelength is shown in Fig. 5(b). The frequency response was measured with two additional laser sources operating at 780 nm and 850 nm. For $C_{fb} = 0$, the maximum achievable bandwidths were 610 MHz (780 nm) and 100 MHz (850 nm). The drop of the bandwidth compared to the response at 675 nm is because of the light penetration depth increases with the wavelength; for higher wavelengths penetration depth becomes comparable or exceeds the absorption zone depth, allowing for slow carrier diffusion from the p-substrate to contribute to the primary photocurrent. The 675-nm wavelength penetration depth falls well into the absorption zone where drift of the carriers occurs, which is a much faster process than carrier diffusion. Therefore, the receiver is best suited for visible 675 nm wavelength.

3.2 Optical Sensitivity of 800APD OEIC

The optical sensitivity is the minimum average optical power necessary to obtain a certain bit-error-ratio (BER). The laser source was in this case modulated via bit pattern generator at different data rates using the pseudo-random binary sequence (PRBS) of length 2^{31}–1. The fiber was again coupled to the photodiode active area and the receiver output was fed into the bit-error tester to count the BER. The target BER was set to 10^{-9} which is a standard value in the fiber optics community. The sensitivity curves at four different data rates are shown for the case of maximum bandwidth in Fig. 6(a) when $C_{fb} = 0$ and in case when a feedback capacitance was applied in Fig. 6(b), thus reducing the bandwidth and therefore the overall noise. In case of the applied feedback capacitance, a sensitivity improvement could be noticed for lower data rates. Table 2 summarized the achieved results. The achieved sensitivity at 1 Gbit/s of – 33 dBm is close to the sensitivity of the hybrid APD receiver reported in [2] which reached a sensitivity of

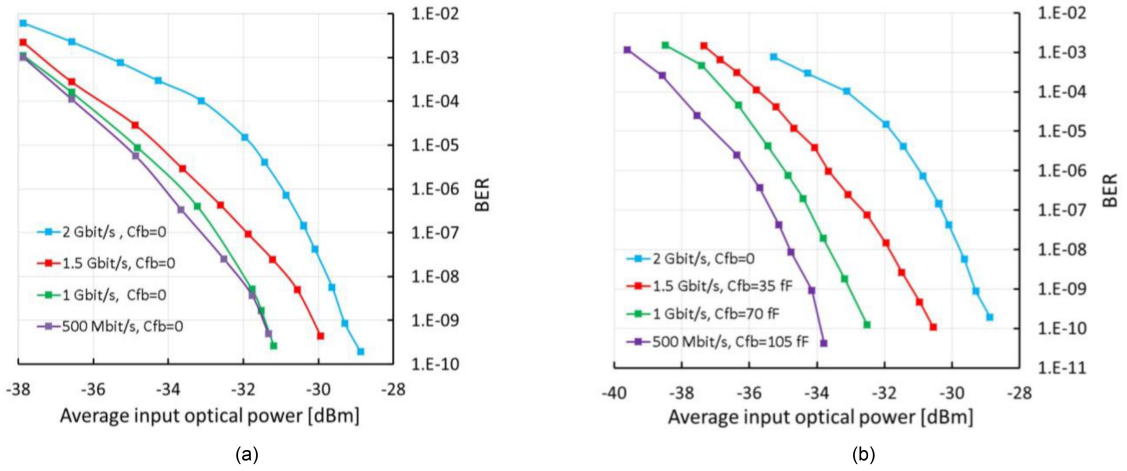

Fig. 6. Optical sensitivity of the 800APD OEIC: a) without applied Cfb and b) with different values of Cfb.

TABLE 2
Summary of Measured Optical Sensitivities of the 800APD OEIC at Different Data Rates

Receiver	Data rate	C_{fb}	V_{sub}	M	Sensitivity
800 APD OEIC	500 Mbit/s	0	-57 V	23.4	-31.4 dBm
	1 Gbit/s	0	-57 V	23	-31.4 dBm
	1.5 Mbit/s	0	-56.5 V	21	-30.1 dBm
	2 Gbit/s	0	-57 V	23.6	-29.3 dBm
	500 Mbit/s	35 fF	-56.5 V	21	-34.1 dBm
	1 Gbit/s	70 fF	-56.5 V	22	-33 dBm
	1.5 Gbit/s	105 fF	-56 V	21	-31 dBm

–35 dBm at 1.25 Gbit/s but had a smaller APD diameter of 500 μm. Since the diameter of the photodiode, i.e., the active area, is proportional to the photodiode capacitance, having large active photodiode area and obtaining a high sensitivity at the same time is very challenging. Therefore, the integrated approach proved more than comparable to the hybrid one [2] which used a noise optimized commercially available APD wire-bonded to a high-speed TIA circuit (AD500-1.3G-TO5) with breakdown voltage at 160 V.

A comparison with fully integrated optical receivers is also provided. Table 3 summaries the sensitivities of the fully integrated linear receivers in both CMOS and BiCMOS technologies that are not solely intended for fiber communication i.e., having large photodetection areas suitable for optical wireless communication. The minimum detection area in the Table 3 is 70 $\times$ 70 μm^2, therefore larger than the multimode fiber diameter with typical radius of 62.5 μm. From Table 3 it can be seen that the APD receivers outperform their PIN/P-N counterparts in terms of sensitivity by large margin, however the achievable data rates are lower in some cases. Large feature size technologies can offer better photodiode properties reflected in low-field responsivity R ($M = 1$) which is directly influenced by the thickness of the depletion layer. The small-feature-size CMOS receivers can achieve high data rates and are compatible with down scaling trend tailored for digital electronics, but they suffer from rather poor sensitivities. The receiver described in this work falls well into the state of art sensitivities especially considering that it has one of the largest light-sensitive areas.

TABLE 3
Fully Integrated Linear APD and PIN Receivers With Large Photodetection Areas (in Case of APDs, for R the Low-Field Value is Given i. e. M = 1)

Ref	Technology	PD	λ[nm]	R [A/W]	Area [μm^2]	Data rate	Sensitivity
[19]	0.6 μm BiCMOS	PIN	660	0.36	74 558	2.5 Gbit/s	-20.1 dBm
[20]	0.5 μm BiCMOS	PIN	660	0.5	13 2548	1.25 Gbit/s	-23 dBm
[21]	0.35 μm HV CMOS	APD	675	0.41	31 400	1 Gbit/s	-31.8 dBm
[22]	0.35 μm HV CMOS	APD	675	0.46	125 600	1 Gbit/s	-34.7 dBm
[7]	0.35 μm BiCMOS	APD	675	0.435	31 400	1 Gbit/s	-35.5 dBm
						2 Gbit/s	-32.2 dBm
[8]	0.35 μm BiCMOS	APD	675	0.445	125 600	1 Gbit/s	-34.6 dBm
						2 Gbit/s	-30.6 dBm
[23]	0.35 μm BiCMOS	PIN	675	0.54	33 113	3 Gbit/s	-23.4 dBm
[24]	0.18 μm CMOS	P-N	660	0.21	785 000	0.6 Gbit/s	-10.65 dBm
[25]	0.18 μm CMOS	P-N (SML)	850	0.052	5 625	5 Gbit/s	-3.67 dBm
[26]	0.13 μm CMOS	P-N (SML)	850	0.05	4 900	8.5 Gbit/s	-3.87 dBm
[27]	65 nm CMOS	P-N	670	0.36	62 500	4 Gbit/s	-3 dBm
This work	0.35 μm BiCMOS	APD	675	0.45	502 400	1 Gbit/s	-33 dBm
						2 Gbit/s	-29.3 dBm

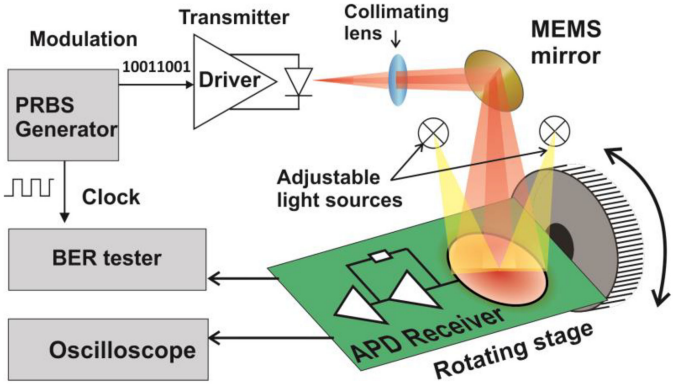

Fig. 7. 800APD OEIC as a receiver element in OWC.

4. VLC Experiments

The setup for VLC experiments is presented in Fig. 7. The designed APD receiver was mounted on a rotating stage on one end of the laboratory room, while the transmitter could be placed at various distances. The average optical output power was measured to be 0.85 mW at 680 nm, the laser source was a vertical cavity surface emitting laser (VCSEL) driven by a commercial driver from Maxim (MAX3740A). The output light beam was collimated with an inexpensive lens from Roithner (MPG-95) to a beam divergence of 0.057° (FWHM). The transmitter was driven via a bit pattern generator at 1 Gbit/s and 2 Gbit/s. The receiver outputs were fed to the oscilloscope to obtain eye diagrams and to the bit-error tester. The rotating stage on which the receiver was mounted enabled the measurements of the influence of angle displacement on BER. The additional adjustable light sources were used for emulating ambient light conditions. During the measurements, there was no optics in front of the APD receiver to increase the collection area, and there was no interference filter to reduce the influence of background ambient lighting.

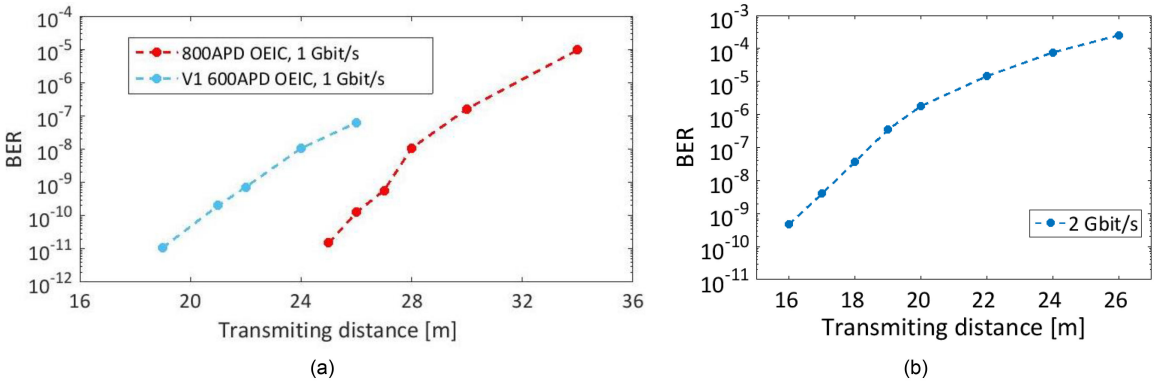

Fig. 8. Measured BER vs. transmission distance at (a) 1 Gbit/s, and (b) 2 Gbit/s.

4.1 Maximum Error-Free Transmission Distance

The maximum error-free (BER $< 10^{-9}$) transmission distance for 1 Gbit/s was 27 m, see Fig. 8(a), measured under normal ambient lighting of the lab facilities used. The calculated signal irradiance at this distance is 1.5 μW/mm^2. For comparison, an APD receiver designed in the same technology but optimized for a 600-μm diameter APD published in [18] was also measured in the same OWC setup and achieved 22 m at 1 Gbit/s, requiring an irradiance of 2.26 μW/mm^2. The version of the 600-μm diameter APD receiver (V1 600APD OEIC) from [18] incorporated the dc current rejection loop proposed in [28]. This dc current rejection loop cancels the dc current component from the signal, but as well the dc current originating from the unwanted ambient light so that this dc currents do not change the bias points in the circuit. Nevertheless, the 800APD OEIC still outperformed the V1 600APD OEIC due to its larger active area that reduces the needed irradiance 1.5 times.

In [29] an OWC experiment in indoor settings up to 1.5 m at data rates up to 3 Gbit/s were reported and in outdoor setting up to 72 m at data rates up to 2 Gbit/s [30]. The work in [30] used an APD also in a standard 0.35 μm CMOS process but it was not fully integrated with TIA circuit. Instead, a low-noise amplifier (LNA) was ac-coupled to a wire bonded APD fabricated in CMOS. The standard CMOS APD together with external LNA reached data rates up to 1-2 Gbit/s and the needed average optical power without the gain of the optical elements was estimated to –30 dBm for a target BER at the FEC limit ($3.8{\cdot}10^{-3}$). The CMOS APD receiver operated at the same wavelength of 680 nm as the APD receiver in this work. The APD had an area of 100 μm $\times$ 100 μm which needed to be segmented to reach the high speed; the active area of that device is 50.2 times smaller than the active area of 800APD OEIC from this work. Additionally, if the FEC limit would be used as BER limit in this work, the sensitivity would improve by approximately 6 dB (to –35.3 dBm) at 2 Gbit/s and by 5.5 dB (to –38.5 dBm) at 1 Gbit/s, thus outperforming the APD receiver from [29], [30] by large margin. The reached transmission distances in [30] were enabled by use of large area collecting optics (50–70 mm diameter) at both receiver and transmitter side. Here, we aimed at a lens-less operation for wide-field-of-view FoV at receiver side, to make a case for an easy-to-assemble, compact and cost-effective APD receiver intended for OWC.

The BER dependence on transmission distance was also tested for an increased data rate of 2 Gbit/s for the 800APD OEIC as receiver, see Fig. 8(b). The maximum reachable distance was 16.5 m for BER $= 10^{-9}$. The achieved maximum transmission distance values are higher than in case of the APD receivers in the same BiCMOS technology which did not use modulation doping with APD diameters of 200 μm and 400 μm [31], [32], and which had a k_{eff} of 0.0789 thus offering better APD noise performance. These receivers were tested in the same VLC measurement setup. Despite these receivers having a better APD noise performance, the 800APD OEIC outperformed them in transmission reach due to the high collection area. Fig. 9 shows eye diagrams at 1 Gbit/s at 25 m of transmission distance and 2 Gbit/s at 16 m of transmission distance.

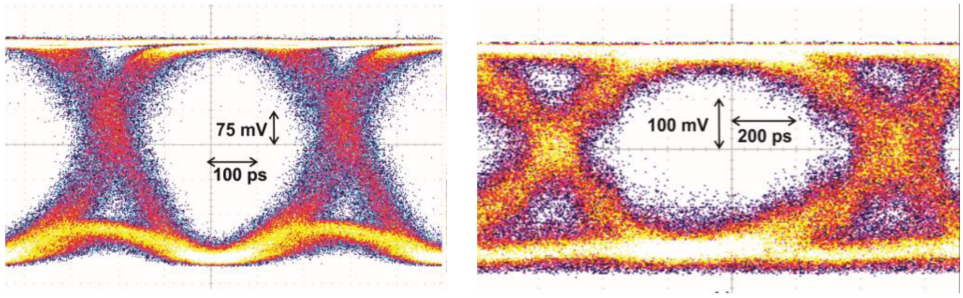

Fig. 9. Measured eye diagrams at (a) 2 Gbit/s, 16 m of transmission distance and (b) 1 Gbit/s, 25 m of transmission distance.

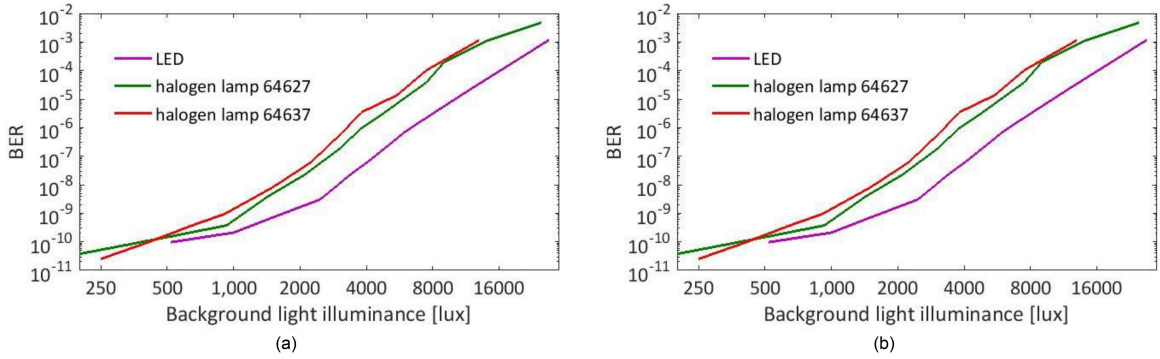

Fig. 10. (a) BER using the 800APD OEIC as receiver at 1 Gbit/s vs. illuminance of ambient light sources. (b) BER using different APD OEICs at 1 Gbit/s vs. illuminance of halogen lamp 64637.

4.2 Background Light Interference

With increased photodiode active area, not only the collected signal power is increased but also is the collected ambient light optical power. The generated dc background photocurrent is a source of shot noise which is very detrimental to APD receivers since it is amplified by the internal APD gain together with the signal. In [22], the optical spectrum of the artificial light sources measured with an AvaSoft spectrometer is given; additionally, for reference, a lab lighting spectrum is also provided. The lab lighting has a fluorescent spectrum which is commonly found in indoor facilities, especially industrial ones [33]. The additional light sources were two OSRAM halogen lamps (halogen lamp 64627 and halogen lamp 64637) and one white LED lamp. All three of these additional light sources have a quite continuous spectrum, and the halogen lights have strong emission in the wavelength range from 500–700 nm which coincides with the responsivity curve of the APD in this technology [13]. Therefore, these light sources emulate almost the worst-case conditions, especially given the fact that these were directly pointed onto the receiver without any shadowing. The illuminance levels were measured with a lux meter in front of the receiver.

Prior to background light variation, the transmitter was placed at the distance of 25 m where BER value was lower than 10^{-9} to top the signal above the initial error-free margin. At this distance the BER level was comparable to the BER levels in our previous studies [22], [31], [32] when also the influence of the background illuminance was measured. The BER dependence on the illuminance levels of the adjustable background light sources is shown in Fig. 10(a). The biasing voltage was kept fixed at –52 V, which was optimum at low background light levels. At the distance of 25 m, corresponding to signal irradiance of approximately 1.75 μW/mm^2, the allowable lux levels for BER $< 10^{-9}$ were: 1150 lux (halogen light 64627), 950 lux (halogen light 64637) and 1700 lux

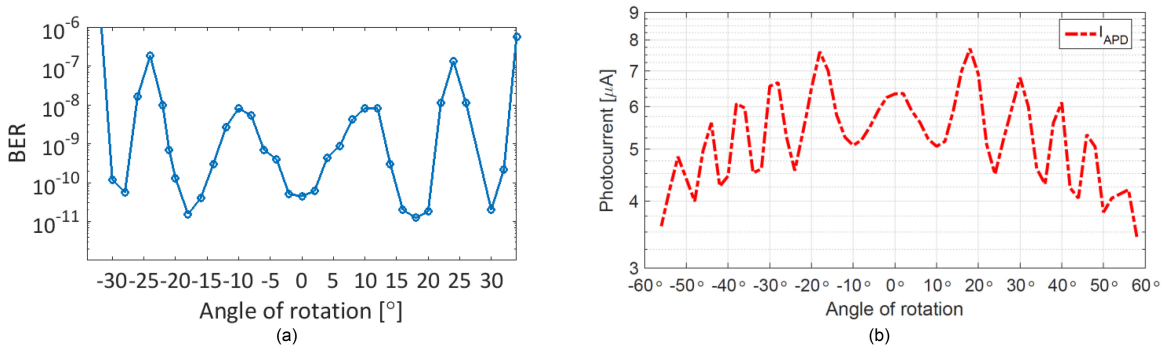

Fig. 11. (a) BER measured at 25 m of transmission distance at 1 Gbit/s vs. receiving angle. (b) Photocurrent vs. angle of rotation.

(LED). The achievable values for these harsh ambient conditions are above of 500 lux which is considered as normal indoor light level [34]. For comparison, V1 600APD OEIC receiver was also tested with halogen light 64637, as well as another version of this chip (V2 600APD OEIC), which had similar properties as the V1 600APD OEIC except the feedback loop which was made identical to the 800APD OEIC. The feedback loop did not influence noise performance, the most important difference is that the dc photocurrent originating from signal as well as ambient light in case of the 800APD OEIC and the V2 600AP OEIC is fed into the TIA and postamplifying stages, therefore changing their dc operating points as it increases. For fair comparison, both 600APD OEICs were operated at 1 Gbit/s and placed at the transmitting distances which allowed for similar starting BER level (at low ambient light); both receivers could work up to higher background light levels compared to the 800APD OEIC, see Fig. 10(b). The main reason for higher tolerable background illuminance is the smaller collection, i.e., photodetection area in the case of the 600APD OEICs. The smaller photodetection area translates into collection of less background radiation thus reducing the additional shot noise which originates from the background dc photocurrent. The V1 600APD OEIC, which had a dc current rejection loop, performed better than the V2 600APD OEIC without the dc rejection loop, which is an expected result since the latter is not experiencing changed operating points of the electrical circuitry. The V1 600APD OEIC could ensure error free data transfer up to 2650 lux compared to 1350 lux in case of the V2 600APD OEIC when the halogen lamp 64637 was used. Therefore, optical receivers for OWC should be designed with the dc rejection loop to make them more background illuminance proof. Additionally, the dc rejection loop can be made entirely on chip without the need for external components as done in [18].

4.3 Field of View

The field-of-view (FoV) is usually defined as the maximum incidence angle at which the optical power can still be received, in [35] the received power limit is set to half of the maximum optical power i.e., FoV is defined based on a 3 dB of power loss. Since our receiver has no optics it is inherently a wide FOV receiver, but with any angular displacement there is a power penalty and the amount of received optical power directly influences the achievable BER. The received optical power P_r for a lens-free receiver follows the cosine law with respect to impinging optical power P_{in} i.e., $P_r = P_{in}\ cos\ \alpha$, where α is the angle between receiver surface normal and optical beam. Fig. 11(a) shows the BER in dependence on the angular displacement. During these measurements the receiver was placed at 25 m and the data rate was 1 Gbit/s. As shown in Fig. 11(a), there exists a trend in decreasing BER with the cosine of the angular displacement between receiver surface normal and transmitter beam – as expected – but with small oscillations. These small oscillations are due to the absence of antireflection coating on top of the APD due to

incompatibility with other mask layers. The stack of different layers on top of the APD acts effectively like an interferometer where depending on the incidence angle a destructive or constructive interference happens resulting in local optical power minima and maxima. These optical minima and maxima can be seen in the variations of generated photocurrent depending on the incidence angle, see Fig. 11(b). The photocurrent minima translate to higher BER values due to loss of signal power. For an error-free transmission (BER $= 10^{-9}$) at 25 m distance an angular tilt of $\pm$ 6° could be tolerated. However, if we look at the generated photocurrent Fig. 11(b) it can be seen that it does not drop below its half-maximum value (3.7 μA) even over very wide angle of approximately $\pm$60° and even at such high tilting angles the achieved BER was $9{\cdot}10^{-4}$ which is still below the FEC limit of $3.8{\cdot}10^{-3}$ [36]. The final useful FoV would therefore depend on the target BER.

4. Conclusion

The work describes the development and experimental characterization of a fully integrated 800 μm diameter APD OEIC in a standard 0.35 μm BiCMOS process that requires no process modifications. To the best of the authors' knowledge, this is the APD OEIC with the largest active area published so far. The large-area APD receiver is appropriate for data rates up to 2 Gbit/s, offering high sensitivities which are comparable to hybrid APD receivers which profit from the high performance of commercial APDs. The receiver was used in VLC setup, where its large collection area enabled a high transmission distance of 27 m at 1 Gbit/s without using any optics at the receiver side. The influence of different ambient light sources was also investigated without using any filtering at the receiver side, thus putting into perspective the impact of the used ambient light source if the low-cost filter-free APD receiver is to be used. By comparing the 800-μm diameter APD receiver in this work to the 600-μm diameter APD receiver from [18], the reduced needed irradiance that come with increased collection area of the APD are leveraged against the reduced optical sensitivity and higher level of collected ambient light that also comes with increased APD area. The maximization of the APD diameter has clear benefits for OWC performance for these single channel receivers even in the presence of background light when no filtering is used. Additional insight for future design is the importance of the dc current cancelation loop which can help in combating ambient light conditions. The maximum APD diameter in this technology could be further increased, but the hard limit for Gbit operation would be set by the circuit design constraints such as transimpedance gain and allowable power consumption.

References

[1] European project ICT-317669-METIS, deliverable D8.4 METIS final project report, Apr. 2015. [Online]. Available: https://www.metis2020.com/documents/deliverables/METIS_D8.4_v1.pdf
[2] D. O'Brien *et al.*, "High-speed optical wireless demonstrators: Conclusions and future directions," *IEEE J. Lightw. Technol.*, vol. 30, no. 13, pp. 2181–2187, Jul. 2012.
[3] V. Jungnickel, A. Forck, T. Haustein, U. Krüger, V. Pohl, and C. von Helmolt, "Electronic tracking for wireless infrared communications," *IEEE Trans. Wireless Commun.*, vol. 2, no. 5, pp. 989–999, Sep. 2003.
[4] A. Borkute and A. Padole, "(Light fidelity) — The future technology in wireless communication," *Int. J. Scientific Eng. Res.*, vol. 4, no. 12, pp. 153–161, 2013.
[5] M. Wolf, J. Li, L. Grobe, D. O'Brien, H. L. Minh, and O. Bouchet, "Challenges in GBPS wireless optical transmission," in P. Chatzimisio, C. Verikoukis, I. Santamaría, M. Laddomada, and O. Hoffmann O. (eds), in *Mobile Lightweight Wireless Systems, Mobilight 2010. Lecture Notes of the Institute for Computer Sciences, Social Informatics and Telecommunications Engineering*, vol. 45. Springer, Berlin, Heidelberg, 2010, pp. 484–495.
[6] S. Ray, M.M. Hella, M.M. Hossain, P. Zarkesh-Ha, and M.M. Hayat, "Speed optimized large area avalanche photodetector in standard CMOS technology for visible light communication," in *Proc. IEEE Sensors*, Valencia, Spain, Nov. 2014, pp. 2147–2150.
[7] T. Jukić, B. Steindl, R. Enne, and H. Zimmermann, "200 μm APD OEIC in 0.35 μm BiCMOS," *IEEE Electron. Lett.*, vol. 52, no. 2, pp. 128–130, Jan. 2016.
[8] T. Jukić, B. Steindl, and H. Zimmermann, "400 μm diameter APD OEIC in 0.35 μm BiCMOS," *IEEE Photon. Techol. Lett.*, vol. 28, no. 18, pp. 2004–2007, Sep. 2016.
[9] R. Enne, B. Steindl, and H. Zimmermann, "Speed optimized linear-mode high-voltage CMOS avalanche photodiode with high responsivity," *OSA Opt. Lett.*, vol. 40, no. 19, pp. 4400–4403, 2015.

[10] P. Brandl, R. Enne, T. Jukić, and H. Zimmermann, "OWC using a fully integrated optical receiver with large-diameter APD," *IEEE Photon. Technol. Lett.*, vol. 27, no. 5, pp. 482–485, Mar. 2015.
[11] T. Jukić, "Empfänger mit integrierter lawinenfotodiode [Receiver with integrated avalanche photodiode]," Ph.D. dissertation, TU Wien Inst. Electrodyn., Microw. Circuit Eng., Vienna, Austria, 2017.
[12] B. Steindl, T. Jukić, and H. Zimmermann, "Optimized silicon CMOS reach-through avalanche photodiode with 2.3-GHz bandwidth," *SPIE Opt. Eng.*, vol. 56, no. 11, 2017, paper 110501.
[13] B. Steindl, W. Gaberl, R. Enne, S. Schidl, K. Schneider-Hornstein, and H. Zimmermann, "Linear mode avalanche photodiode with 1-GHz bandwidth fabricated in 0.35- μm CMOS," *IEEE Photon. Technol. Lett.*, vol. 26, no. 15, pp. 1511–1514, Aug. 2014.
[14] T. Jukić, P. Brandl, and H. Zimmermann, "Determination of the excess noise of avalanche photodiodes integrated in 0.35-μm CMOS technologies," *SPIE Opt. Eng.*, vol. 57, no. 4, 2018, paper 044101.
[15] S.S. Taylor and T.P. Thomas, "A 2pA /$\sqrt{}$Hz 622 Mb/s gaas MESFET transimpedance amplifier," in *Proc. IEEE Int. Solid-State Circuits Conf. (ISSCC)*, San Francisco, CA, USA, 1994, pp. 254–255.
[16] Y. Greshishchev and P. Schvan, "A 60 dB gain 55 dB dynamic range 10 Gb/s broadband sige HBT limiting amplifier," in *Proc. IEEE Int. Solid-State Circuits Conf. (ISSCC)*, San Francisco, CA, USA, 1999, pp. 382–383.
[17] C.D. Holdenried, J.W. Haslett, and M.W. Lynch, "Analysis and design of HBT cherry-hooper amplifiers with emitter-follower feedback for optical communications," *IEEE J. Solid-State Circuits*, vol. 39, no. 11, pp. 1959–1967, Nov. 2004.
[18] D. Milovančev, T. Jukić, B. Steindl, and H. Zimmermann, "Optical wireless monolithically integrated receiver with large-area APD and dc current rejection," in *Proc. Adv. Wireless Optical Commun. (RTUWO)*, Riga, Latvia, 2017, pp. 12–16.
[19] R. Swoboda and H. Zimmermann, "2.5 Gbit/s silicon receiver OEIC with large diameter photodiode," *Electron. Lett.*, vol. 40, no. 8, pp. 505–507, Apr. 2004.
[20] W. Gaberl, R. Swoboda, and H. Zimmermann, "Integrated optical receiver for lens-less short range free-space gigabit communication," in *Proc. IEEE 35th Eur. Conf. Optical Commun. (ECOC)*, Vienna, Austria, Sep. 2009, pp. 1–2.
[21] P. Brandl, T. Jukić, R. Enne, K. Schneider-Hornstein, and H. Zimmermann, "Optical wireless APD receiver with high background-light immunity for increased communication distances," *IEEE J. Solid-State Circuits*, vol. 51, no. 7, pp. 1663–1673, Jul. 2016.
[22] D. Milovančev, P. Brandl, T. Jukić, B. Steindl, N. Vokić, and H. Zimmermann, "Optical wireless APD receivers in 0.35 μm HV CMOS technology with large detection area," *OSA Opt. Express*, vol. 27, no. 9, pp. 11930–11945, Apr. 2019.
[23] P. Brandl, S. Schidl, and H. Zimmermann, "PIN photodiode optoelectronic integrated receiver used for 3-Gb/s free-space optical communication," *IEEE J. Sel. Topics Quantum Electron.*, vol. 20, no. 6, pp. 391–400, Nov./Dec. 2014.
[24] F. Tavernier and M. Steyaert, "High-speed POF receiver with 1 mm integrated photodiode in 180 nm CMOS," in *Proc. IEEE 36th Eur. Conf. Opt. Commun. (ECOC)*, Torino, Italy, Sep. 2010, pp. 1–3.
[25] T. S. Kao, F. A. Musa, and A. C. Carusone, "A 5-Gbit/s CMOS optical receiver with integrated spatially modulated light detector and equalization," *IEEE Trans. Circuits Syst. I: Regular Papers*, vol. 57, no. 11, pp. 2844–2857, Nov. 2010.
[26] D. Lee, J. Han, G. Han, and S. M. Park, "An 8.5-Gb/s fully integrated CMOS optoelectronic receiver using slope-detection adaptive equalizer," *IEEE J. Solid-State Circuits*, vol. 45, no. 12, pp. 2861–2873, Dec. 2010.
[27] Y. Dong and K. W. Martin, "A 4-Gbps POF receiver using linear equalizer with multi-shunt-shunt feedbacks in 65-nm CMOS," *IEEE Trans. Circuits Syst. II*, vol. 60, no. 10, pp. 617–621, Oct. 2013.
[28] K. Phang and D.A. Johns, "A CMOS optical preamplifier for wireless infrared communications," *IEEE Trans. Circuits Syst. II: Analog Digit. Signal Proc.*, vol. 46, no. 7, pp. 852–859, Jul. 1999.
[29] B. Fahs and M.M. Hella, "3 Gb/s OOK VLC link using bandwidth-enhanced CMOS avalanche photodiode," in *Proc. Opt. Fiber Commun. Conf. Exhib. (OFC)*, Los Angeles, CA, USA, 2017, pp. 1–3.
[30] B. Fahs, M. Romanowicz, and M.M. Hella, "A GBPS building-to-building VLC link using standard CMOS avalanche photodiodes," *IEEE Photon. J.*, vol. 9, no. 6, 2017 Art. no. 7907709.
[31] D. Milovančev, T. Jukić, P. Brandl, B. Steindl, and H. Zimmermann, "OWC using a monolithically integrated 200 μm APD OEIC in 0.35 μm BiCMOS technology," *OSA Opt. Exp.*, vol. 24, no no. 9, pp. 918–923, 2016.
[32] D. Milovančev, T. Jukić, P. Brandl, B. Steindl, and H. Zimmermann, "Optical wireless communication using a fully integrated 400 μm diameter APD receiver," *IET J. Eng.*, vol. 8, pp. 506–511, 2017.
[33] J. Quill, G. Fedor, P. Brennan, and E. Everett, "Quantifying the indoor light environment," Q-Lab corporation, *Tech. Bull.*, 2007.
[34] H. Juslén, "Lighting, productivity and preferred illuminances: Field studies in the industrial environment," Ph.D. dissertation, Dept. Elect. Commun. Eng., Helsinki University of Technology, Lighting Laboratory Espoo, Finland 2007.
[35] M. Bertrand, O. Bouchet, and P. Besnard, "Personal optical wireless communications: LOS/WLOS/DIF propagation model and QOFI," in *Proc. Int. Symp.. Commun. Syst., Netw. Digit. Signal Proc. (CSNDSP)*, Graz, Austria, 2008, pp. 179–182.
[36] ITU-T Recommendation G.975.1, 2004, Appendix I.9.